Magma differentiation and contamination: Constraints from experimental and field evidences

A. Castro[1], C. Rodríguez[2, 3], J. Díaz–Alvarado[2], C. Fernández[2], O. García–Moreno[4]

[1]Institute of Geosciences, Consejo Superior de Investigaciones Científicas, CSIC–UCM, Ciudad Universitaria, 28040 Madrid, Spain,
[2]Departamento de Ciencias de la Tierra, Universidad de Huelva, 21071, Spain,
[3]ICT, Departamento de Geociências, ECT, Universidade de Évora, 7000–671, Portugal,
[4]Departamento de Geología, Universidad de Oviedo, 33005, Spain.

Corresponding author: Antonio Castro (antonio.castro@csic.es)

Keywords: Experimental petrology, fractionation, magma contamination, Magma crystallization, batholiths

Abstract

Differentiation and contamination of silicic magmas are common phenomena characterizing the granite batholiths and large igneous provinces that build up most of the continental crust. Although they can be identified by means of geochemical relations of igneous rocks exposed in the continents, the mechanisms allowing magmas to undergo the necessary crystal–liquid separation and digestion of country rocks for differentiation and contamination are poorly constrained. In this paper we show two independent approaches that are essential to understand fractionation and contamination of magmas. These are (1) the study and interpretation of field relations in exposed deep sections of batholiths, and (2) the results of laboratory experiments carried out at middle–upper crust pressure. Experiments support that fractionation is intrinsic to crystallization of water-bearing magmas in thermal boundary layers created at the sidewalls of ascent conduits and walls of magma chambers. Gravitational collapse and fluid migration are processes identified in experimental capsules. Similarly, reaction experiments in mixed capsules support reactive bulk assimilation as a plausible mechanism that is compatible with field and petrographic observations in contaminated granitic rocks.

1 Introduction

Magmatic fractionation (closed system) and contamination (open system) are common processes involved in the overall differentiation of igneous rocks in the continental crust [*Bowen*, 1928]. The two processes can act jointly in magma chambers and conduits. Many silicic (SiO_2 > 53 wt%) igneous rocks, in particular those formed in active continental margins, can be modeled geochemically as resulting from a combination of assimilation and fractional crystallization (AFC) [*Bohrson and Spera*, 2001; *DePaolo*, 1981]. However, the relative contribution of each process and the mechanisms of operation in magmas remain unconstrained.

Many igneous rocks appearing in the continental crust, and particularly those richer in SiO_2, contain isotopic signatures indicating contamination with older crustal rocks [*Allègre and Ben Othman*, 1980; *Hawkesworth and Kemp*, 2006; *Kemp et al.*, 2007; *McCulloch and Wasserburg*, 1978]. Contamination may be acquired either during

ascent and emplacement in the crust, or may be inherited from an already crustal-contaminated source. Trace elements and isotopic ratios, which are regularly used to make AFC modeling, are unable to discern between the two processes. Fortunately, the major element compositions of melts are dependent on the composition of the solid saturation assemblage, which is in turn imposed by intensive variables in a given system, in such a way that the composition of melts in closed systems will follow cotectic lines that can be determined by means of phase equilibrium experiments and thermodynamic modeling. Comparisons between rocks and experimental liquids may help to distinguish open from closed magmatic systems. It is expected that open system processes may introduce characteristic departures in the composition of rocks from that of cotectic liquids. In a theoretical case, rocks belonging to a magma fractionation series will represent liquids extracted at any time in the course of crystallization. These are the so-called *liquid lines of descent* (LLD) [*Bowen*, 1928]. However, in practice, rock series may depart from the ideal composition of LLDs, even in case that the system is closed. The reason is that the extracted liquid fraction may carry magmatic crystals in suspension from a magma chamber or may drag crystals from the consolidated parts of the chamber or conduits in the way upward. These are self-contaminated liquids (Fig. 1). Similarly, the crystal rich residue left after a partial extraction of melt becomes a new magma system that neatly departs form the cotectic. This is a very common case in granitic rocks, in which a residual liquid escaped in the course of crystallization. These are called *disguised cumulates [Lee and Morton, 2015]*, as a cumulate texture is not recognized while an off-cotectic composition is identified. Magmatic differentiation by crystal fractionation is possible if either a liquid fraction is removed from the crystallizing magma or a fraction of crystals is separated away from the magma. Both process differ significantly each other and can operate under different circumstances. The virtual absence of monomineralic layering in silica-rich calc-alkaline systems, indicate that crystal settling is not a dominant mechanism.

Understanding how crystals and liquids are separated in crustal magmas requires special attention to physical and chemical features of crystallizing magmas. Most crustal magmas are characterized by high silica contents. The implication is that viscosity is much higher than that of basaltic magmas, making crystal–liquid separation difficult to achieve [*Glazner*, 2014]. However, many lines of evidence, mostly supplied by geological and geochemical relations, point to an effective fractionation in nearly closed magma systems. Solution to this paradox has been addressed by several approaches,

including numerical modeling [*Bachmann and Bergantz*, 2004; *Bachmann and Huber*, 2016; *Burgisser and Bergantz*, 2011; *Gelman et al.*, 2014], analog experiments [*Michioka and Sumita,* 2005; *Shibano et al.,* 2012; 2013] and experiments with silicate melts at high pressure and high temperature (*Masotta et al.* [2012]; *Huang et al.* [2009]; *Rodríguez and Castro* [2017]). Magma crystallization in a thermal boundary layer (TBL), created for instance at the walls of magma chambers and conduits [*Rodríguez and Castro*, 2017], is the most plausible mechanisms that contributes to separation of liquids from crystals within a solidification front [*Marsh*, 2002].

Because assimilation is usually considered an energy-consuming process, its role in accounting for significant differentiation of igneous rocks has been questioned [*Bowen*, 1922; *Glazner*, 2007; *Thompson et al.*, 2002]. Energy balance is applied in terms of xenolith melting and, thus, assimilation is considered as a particular case of magma mixing [*Thompson et al.*, 2002] between melts from the xenoliths and the intruding magma. Also limiting is the assumed low temperature for the country rocks to be assimilated [*Glazner*, 2007]. However, the reach of assimilation, far from being a self-limiting process, can be enlarged in cases of hot country rocks and repeated intrusions of magma [*Glazner*, 2007]. In addition, country rock xenoliths can be disaggregated mechanically by inducing melting at low melt fractions, contributing to the so-called *reactive bulk assimilation* [*Beard et al.*, 2005] in which energy consume is minimized. The observation of contaminated rocks over kilometric extensions of plutonic intrusions from the Variscan Gredos batholith in Central Spain, which were emplaced in repeated layers into migmatitic metasediments [*Díaz–Alvarado et al.*, 2011], points to country rock assimilation as an efficient mechanism that contributes to differentiation of magmas in the continental crust. These areas provide relevant field relations that may help to understand the intricacies of assimilation. A summary of these relations is shown in this paper.

In regard of the mechanisms of assimilation, essential questions are: How is in detail the process of assimilation? How do exotic elements incorporate to the magmas? What is the scope of assimilation in nature? Answering these questions require a knowledge of the process. Although some geochemical features may be indicative of magmatic assimilation, the study of field relations between igneous intrusions and country rocks in deep-seated plutons is essential to reveal the mechanisms of magma–host interactions. Even in field-based examples, the intricacies of the processes of magma–host interaction leading to contamination are poorly constrained. Experiments are useful

to set limits to possible processes involving chemical equilibrium and disequilibrium. Integration of petrological phase equilibrium relations and field-based studies are essential to discern between competing processes. Furthermore, the identification of paleotectonic environments through the geochemistry of magmas requires a wholly understanding of petrogenetic processes, contamination being a very common one and, at the same time, the most difficult to reveal. At this purpose, we present new field description from the Gredos batholith (Central Spain) that are interpreted in the light of evidences from relevant laboratory experiments on magma differentiation and crustal contamination

2 Geological and Geochemical Inferences on Fractionation

On the basis of geochemical studies, granites of the Cordilleran batholiths are linked to fractionation from an intermediate magma precursor of andesitic to basaltic andesitic composition (e.g., Sierra Nevada batholith [*Lee et al.*, 2006]; Patagonian batholith [*Castro et al.*, 2019; *Castro et al.*, 2011; *Pankhurst et al.*, 1999]). Experimental phase equilibria [*Castro*, 2019 and refs herein] also point to a similar way, adopting an intermediate precursor as the parental magma to batholiths. Even in intracontinental calc-alkaline batholiths (e.g., Caledonian Newer granites and Variscan batholiths of Iberia), whose origin points to fluid-assisted melting of the lower crust (secondary I-type granites) [*Castro*, 2019], a fractionation trend from tonalites and quartz-diorites to granodiorites and granites is observed. Curved patterns in Harker diagrams are characteristic of cotectic variations and, hence, of liquid fractionation from one or various parental magmas. By contrast, rectilinear patterns are considered as indicative of magma mixing or contamination, as they result from a mechanical mixing between two systems, namely magma–host or magma–magma. However, mixing of fractionated liquids with their cognate crystals may also produce rectilinear patterns while the system is closed to external contaminants [*Bea et al.*, 2005]. Figure 1a shows internal mixing relations between liquid and crystals in the MgO–CaO diagram, which can be taken as a proxy of cotectic variations in an ample variety of mafic and intermediate systems, including the calc-alkaline series. The two components, MgO and CaO, are preferentially partitioned into the solid saturating assemblage, which is dominated by Pl+Cpx or Pl–Amp (mineral abbreviations after *Whitney and Evans* [2010]) along a wide temperature interval from near-liquidus to near-solidus conditions. Commonly,

rocks fractionated in closed systems within the continental crust evolve following the curved patterns dictated by the thermodynamic cotectic. However, rock series evolving in a closed system may plot outside the cotectic, as internal mixing between fractionated liquid and crystals from the cumulate is also possible (Fig. 1a). In sum, the geochemical inferences on fractionation must be taken with care. Only curved patterns are indicative of fractionation, as they are governed by thermodynamic cotectic variations. A better way to delimitate patterns of fractionation from those of assimilation is by plotting rocks on triangular diagrams using a multicomponent space projected onto the plane Orthopyroxene–Orthoclase–Anorthite (Fig. 1b).

In calc-alkaline plutonic systems, layered monomineralic cumulates are rare. Paradoxically, plutons are formed by rocks that display nearly-cotectic variations. Thus, where are the cumulates from which fractionated liquids were extracted? The explanation is that fractionation proceeds by expulsion of liquid from a crystallizing magma, and not by separation of crystals from the magma. The resulting cumulates are hardly identified by textures or compositions. Many diorites and gabbros of the calc-alkaline plutonic associations are "disguished" cumulates [*Lee and Morton*, 2015]. That is, they represent crystals aggregates, or mushes, that lost a residual liquid in the course of crystallization. For this reason, rocks of intermediate composition (diorites and quartz-diorites) from batholithic associations are scattered in MgO–silica and MgO–CaO diagrams. These cumulate-like diorites share the same scattered region of lower crust granulites, pointing to fractionation as an overall process responsible for the differentiation of the lower and upper continental crust [*Castro et al., 2013*].

3 Mechanisms of Liquid–Crystal Separation

Although fractionation by liquid–crystal separation is a necessary process to account for geochemical (e.g., cotectic variations in closed systems) and geological (e.g., zoned plutons) observations, the mechanisms of such a physical separation remain debated. Liquid expulsion from a crystallizing aggregate is a preferred mechanism in silicic magmas in which, individual crystal separation by gravity settling is impeded by the high viscosity of melts and the low density contrast between melt and crystals [*Brandeis and Jaupart*, 1986]. However, gravity compaction and expulsion of liquid may be encountered in the crystal-rich mush formed atop of solidification fronts. Also, the interstitial melt trapped in the mush may undergo water saturation leading to boiling and

vesiculation that may force deformation and expulsion of the liquid from a crystalline aggregate. The two processes, gravitational collapse and fluid-assisted filter pressing are analyzed here.

3.1 Gravitational Collapse and Compaction

In spite of the scarce theoretical support to an efficient process of crystal–liquid separation that allows large volumes of silicic magmas to be available in the continental crust in short periods of time [*Bachmann and Huber*, 2018], it is a fact that fractionation is identified on the basis of geochemical nearly-cotectic trends [*Castro*, 2013; *Castro*, 2019], continuous variations in zoned intrusions and large volcanic eruptions of silicic (rhyolitic) magmas [*Lipman*, 1988]. The two main approaches to understand the mechanisms of silicic magma fractionation, namely analog modeling and experimental, have failed to account for the generation of fractionated liquids in the required volumes and at the necessary rate, in a time span shorter than the cooling time in the upper crust. Mechanical interaction of falling particles (crystals) in silicic magmas can occur even at low crystal fractions, leading to a "hindered" settling processes with the implication of slow rates of melt extraction [*Bachmann and Bergantz*, 2004; *Bachmann and Huber*, 2018]. An alternative mechanism is compaction of a crystal-rich matrix, which is considered as effective in increasing the rate of melt extraction [*McKenzie*, 1984]. Compaction is a common phenomenon in long-duration (> 10 days) experimental runs. We discuss below evidences from analog materials and high pressure-high temperature experiments carried out in presence of temperature gradients. These may shed light on the relative importance of gravity settling and compaction in magma chambers.

3.1.1 Analog Experiments and Modeling

Separation of liquid and crystals in the magma chambers was explained in the conceptual and analytical model of *Marsh* [1988] as due to convection beneath the *capture front*, defined as the surface separating the rigid crust and crystal mush layers (crystallinity larger than 25%) from a crystal suspension zone. According to that model, the resulting convection pattern includes crystal-laden plumes falling from the suspension zone to the deeper parts of the chamber. The analog experiments of *Michioka and Sumita* [2005] simulated a solidifying magma chamber by means of an experimental cell consisting of a thin particle layer (glass beads) at the top, overlying a

thick liquid layer (glycerine solution or silicone oil). A limited zone, located at the interface between the particle-rich and the liquid-rich layers, became unstable, forming descending plumes, thereby presenting an experimental confirmation of the convection model of *Marsh* [1988]. The similar analog experiments of *Shibano et al.* [2012] extended those results to the case of a thick particle-rich layer and found that the downwelling crystal-laden plumes actually come from a dilated boundary layer located beneath a granular layer whose particles are in a jammed state. Descent of the plumes caused a cellular convection pattern within the liquid layer, which eroded the dilated boundary layer. This mechanism differs from those of compaction, Stokes settling, hindered settling, and Rayleigh–Taylor instabilities, and permits the upward migration of the liquid layer, becoming a potentially efficient process of melt transport within magma chambers. Interestingly, some of the experiments performed by *Shibano et al.* [2012] do not rule out the activity of permeable flow (compaction and hindered settling) as a secondary mechanism for liquid transport, particularly when the granular layer slides downwards as a whole, allowing the generation of a liquid-rich layer at its top. This mechanism is akin to that described by *Marsh* [2002] to explain the presence of large silicic lenses in the upper part of mafic intrusions. Finally, *Shibano et al.* [2013] advanced in the analysis of magma chamber processes simulating roof melting by means of experimental cells filled with wax and glass beads. Those experiments, which do not preclude the effects of crystallization within the magma chamber, are able to explain the generation of rhythmic layering at the bottom of the chamber, and showed that magma ascent can be a cyclical and intermittent process.

3.1.2 Compaction Experiments at High Pressure–High Temperature

Crystal accumulation is commonly observed in experimental capsules in long-duration runs of several days, overcoming the limitations imposed by the small size of crystals and the expected high viscosity of silica-rich liquids. This phenomenon allows us to simulate experimentally the role of gravity compaction and expulsion of an interstitial liquid from a crystal-rich mush and to compare the results with magmatic differentiation series. In this way, geological inferences and mechanical analysis on a possible collapse of the partially crystallized solidification front atop of magma chambers [*Marsh,* 2002], were confirmed experimentally by *Masotta et al.,* [2012] and contrasted with petrological relations of mush fragments (crystal-rich enclaves) in volcanic rocks

[*Masotta et al.,* 2016]. Another interesting experiment of crystallization, possibly accompanied by compaction, was carried out by *Huang et al*. [2009] using a natural andesite (the AGV USGS standard [*Flanagan*, 1967]) as starting material with added water, crystallizing within a thermal gradient of 600 °C. The favored interpretation was differentiation by ion migration in response to the thermal gradient [*Huang et al*., 2009]. However, the presence of monomineralic crystal layers at the bottom of the capsule indicates that compaction was an effective mechanism of differentiation by crystal–liquid separation in that experiment. It is interesting to mention that experiments with a dry andesite in a thermal gradient (ca. 300 °C) produced no significant differences in composition along the capsule, while marked differences were found in capsules with the same starting material with added water [*Rodríguez and Castro*, 2017]. Thus, the cause of element fractionation must be found in the presence of water and not in the thermal gradient. One of the experiemnts reported by *Rodríguez and Castro* [2017] was carried out with the above mentioned AGV andesite within a 30°C/mm gradient at 5 kbar in the classical vertical position of the piston–cylinder. In this arrangement, identical to the experiment by *Huang et al*. [2009], the thermal gradient within the capsule acts in the same direction than gravity. This vertical experiment was carried out as a benchmark run (Run CRV2; *Rodríguez and Castro* [2017]) to compare with horizontally arranged runs of the same study in which, thermal gradient and gravity are orthogonal (see next section). After comparison, fractionation was less effective compared with horizontal runs as crystal–liquid separation is controlled by gravity compaction and not by exsolution of a strongly fractionated (rich in silica and alkalis) fluid phase within the solidification front (see below). Nevertheless, we found interesting relations in that vertical run that merit the attention here. By contrast with the other thermal gradient experiments, in which temperature remains constant at the hot spot, in the run CRV2 [*Rodríguez and Castro*, 2017] a dynamic thermal gradient is imposed following a programmed cooling ramp of 0.6 °C/hour, representing a more realistic scenario of a cooling magma chamber or dike. A half polished section of the vertical run CRV2 is compared with a horizontal run crystallized under identical conditions but with the gravity vector arranged orthogonal to the gradient temperature vector (Fig. 2). It can be observed that crystals are mostly concentrated at the bottom of the capsule (Fig. 2b) compared with the horizontal run (Fig. 2a). Because both experiments were set at the same initial conditions and both were slowly cooled at the rate 0.6 °C/hour during 309 hours, the only explanation for the observed differences is

compaction and liquid expulsion from the cumulate in the vertical run. Moreover, a thin monomineralic carapace of Amp, the *liquidus* phase of this water-rich system, is broken and collapses down leaving free space near the walls allowing interstitial liquid to scape upwards (Fig. 2e). The upper layer, containing tiny magnetite crystals, is possibly formed during intrusion of upwards moving liquid plumes. The composition of glass (quenched melt) along the capsule is fractionated. In the crystal-free zone, glasses are richer in SiO_2 and K_2O, and poorer in CaO (Fig. 2d) compared with the original composition of the AGV andesite [*Rodríguez and Castro*, 2017]. The constant composition of glasses in the crystal-free zone, within a strong thermal gradient of ~30 °C/mm (see green curve in Fig. 2b) precludes a Soret effect [*Huang et al.*, 2009] as the cause of liquid fractionation. By contrast, these results reinforce the role of gravitational instability as an efficient mechanism to produce liquid–crystal separation. In summary, application of a dynamic thermal gradient enhances fractionation of the bulk magma system accompanied by compaction of the crystal-rich mush formed at the solidification front. Moreover, the results of other compaction experiments [*Huang et al.*, 2009; *Masotta et al.,* 2016] are totally comparable as they are characterized by expulsion from the mush zone (i.e., the side walls of conduits and/or magma chambers) of a fractionated liquid that mixed with the pristine liquid ahead of the front leading to fractionation of the whole system.

3.2 Crystallization in a Vertical (Non-Gravitational) Thermal Boundary Layer (TBL)

The mechanism of compaction and gravitational collapse of a crystal-rich mush requires that the thermal gradient that creates the solidification front is closely parallel to the gravity vector. This condition is satisfied in both the roof and bottom of magma chambers for which, most mechanical models have been developed [*Bachmann and Bergantz*, 2004; *Lake*, 2013; *Marsh*, 2002]. However, the processes of magma crystallization at the vertical walls of magma chambers and the sidewalls of ascent conduits have received less attention [*Humphreys and Holness*, 2010; *Namur et al.,* 2013]. The case of vertical conduits are relevant as most intermediate magmas (e.g., calc-alkaline batholiths) that feed plutons at the upper crust have traveled tens of km from the source region of melt segregation at the lower crust or the upper mantle. In case of horizontal thermal gradients, as the sidewalls of conduits, the alternative to hindered settling and gravitational collapse is liquid expulsion by *gas-driven filter pressing* [*Pistone et al.*, 2015].

3.2.1 Effects of Volatile Exsolution

Rodríguez and Castro [2017] demonstrated experimentally that *gas-driven filter pressing is a* mechanism able to operate in a water-bearing magma crystallizing in a thermal boundary layer (TBL) in which, a continuous variation in the crystal fraction or crystallinity (X_c=crystals/crystals+liquid) from all-solid ($X_c = 1$) to all-liquid ($X_c = 0$) is established. Other properties, as magma viscosity and strength, also changes across the TBL, making the walls of magma conduits and chambers places of special relevance in the generation of textural heterogeneities in magmas [*Fernández and Castro*, 2018]. In this section, only the petrological consequences of gas expulsion and vesiculation by second boiling are explored on the basis of laboratory experiments [*Rodríguez and Castro*, 2017].

The principle is that any water-bearing liquid, the general case of calc-alkaline magma systems, will reach saturation by second boiling in the course of crystallization, in the way as water is partitioned into the remaining liquid, reaching saturation at a given state of crystallinity. The value of X_c for boiling depends on the initial water content (in wt% H_2O) of the magma (W_0) and the water solubility at the pressure of crystallization $[W_s]_{(P)}$. The fraction of water-saturated liquid (X_{sl}) is given by the expression:

$$X_{sl} = W_0 / [W_s]_{(P)} \quad (1)$$

Water solubility is strongly dependent on pressure and weakly on temperature [*Burnham*, 1979]. A relation between pressure and solubility is obtained by second order polynomial regression of the Burnham´s solubility curve for granite liquids [*Castro*, 2013]:

$$W_s = -0.27\,P^2 + 3.54P + 0.42; \text{ (for } P < 6 \text{ kbar)} \quad (2)$$

By substitution in Eq. (1) we get the empirical relation:

$$X_{sl} = W_0 / -0.27\,P^2 + 3.54P + 0.42; \text{ (for } P < 6 \text{ kbar)} \quad (3)$$

From this relation it is possible to know the critical crystallinity ($X_{cc} = 1 - X_{sl}$); That is, the crystal fraction at which the remaining liquid reaches saturation. The value of X_{cc}

depends on the pressure of crystallization and the initial water content of magmas (Fig. 3). The effectiveness of boiling and vesiculation in promoting liquid expulsion and fractionation depends on the rheological state of the partially crystallized magma at the time of water saturation. At relatively high crystallinity ($X_{cc} > 0.7$), deformation of the rigid crust is impeded by the crystal interlocking structure of the magma. Formation of tension gashes can be formed at this state [*Fernández and Castro*, 2018]. Many aplites and pegmatites in granite plutons are true *degassing* structures. These form dikes and irregular pods in which the contacts with the host granite are at the scale of crystals, denoting that the host was a crystal-rich magma, and not a solid rock, at the time of fracturing and fluid segregation. It can be expected that fluids expelled out via fractures (dikes) from the rigid crust of a solidification front, will carry strongly fractionated components that may mix and/or dissolve into the liquid-rich area ahead of the saturation front. Such a mechanism of "fluid migration" is very efficient in granitic magmas giving rise to zoned intrusions and fractionated cupolas atop of plutons. This principle is the basis for crystallization experiments of a water-bearing magma in a thermal gradient (see below).

Depending on the initial water content and the pressure of crystallization, the magma can reach water saturation at varied crystal contents and, thus, varied rheological states within the saturation front can be found [*Rodríguez and Castro*, 2017; *Fernández and Castro*, 2018]. The most favorable state is that of a deformable mush in which the formation of bubbles can push liquid away of the crystal framework by promoting compaction of the crystal aggregate [cf. *Bachmann and Huber*, 2018]. In the case of the sidewalls of conduits, shear deformation of the solidification front may favor liquid expulsion by compaction of the mush. Many flow structures with high concentration of K-feldspar crystals can be explained by this mechanism. Outside the mush zone, in the suspension zone ($X_c < 0.25$), flow is controlled by the liquid phase as crystals are "floating" in the liquid with scarce mechanical interactions. Moreover, water saturation can only be reached in the suspension zone in anomalous cases of high initial water contents and very low pressure (Fig. 3). For a magma to reach saturation at $X_c < 0.5$ at the pressure of 3 kbar, the initial water content must be higher than 6 wt% H_2O.

The most favorable mechanical conditions for water saturation and vesiculation to effectively promote the expulsion of liquid from the crystalline framework, are found within the rigid crust ($X_{cc} > 0.55$), within a critical zone of X_{cc} from 0.6 to 0.7, for magmas with initial water content $W_0 > 3$ wt% [*Pistone et al.*, 2015]. These critical

conditions can be encountered within a wide range of pressure from 3 to 6 kbar (Fig. 3). For shallower conditions ($P < 2$ kbar), low initial water contents ($W_0 < 3$ wt%) are required to get X_{cc} within the critical zone of rigid crust of a solidification front. In sum, the rheological state of the magma must be deformable at the time of melt water saturation to promote liquid expulsion. At values of $X_{cc} > 0.7$ the rigid crust can experience hydraulic fracturing and segregation of a water-saturated melt.

3.2.2 Magma Splitting in a TBL: An Experimental Finding with Implications

The sidewalls of magma ascent conduits represent large transient interfaces along which magma looses heat to the surrounding host with the consequent generation of thermal boundary layers (TBL) along several tens km from the region of magma segregation to the final level of emplacement. It is inferred that these large TBL structures play an important role in magma differentiation during ascent; particularly in the case of water-bearing magmas as water saturation will be encountered within the TBL. All phenomena referred to above in the previous section can operate along the conduits. The main inference for differentiation in TBL at the conduits comes from the presence of autoliths in granite (sensu lato) plutons. It has been demonstrated that most mafic microgranular enclaves characterizing calc-alkaline batholiths are true autoliths and not fragments from synplutonic dikes [*Paterson et al*., 2016; *Žák and Paterson*, 2010]. Autoliths represent eroded fragments from different parts of the TBL (chilled margins) of conduits. All textural observations in autoliths, as the fine-grain size, the presence of resorbed crystals of plagioclase, the presence of double enclaves, together with the observed geochemical and isotopic features [*Rodríguez and Castro*, 2019], are supporting such an interpretation. A mechanical analysis of the rheology of conduits at the TBL accounts satisfactorily for the observed field relations, shape and size of autoliths [*Fernández and Castro*, 2018].

Rodríguez and Castro [2017] carried out experiments to simulate the crystallization of a water-bearing magma in a vertical TBL representing the sidewalls of conduits. The results constituted a significant finding: The liquid ahead of the solidification front is fractionated only if water is present as an initially dissolved phase in the magma [*Rodríguez and Castro*, 2017]. Under identical conditions, runs with dry compositions produced no differentiation effect on the liquid phase. Other interesting result is the sharp boundary between the crystalline zone (the solidification front) and the liquid. The consequence is that a water-bearing magma splits into two systems with a

compositional jump. One system is a differentiated liquid and the other is a crystal-rich mush (Fig. 4). The latter is comparable to natural autoliths [*Rodríguez and Castro*, 2019].

In sum, differentiation in a TBL is interpreted as the result of liquid expulsion from the solidification front in the course of crystallization and water saturation. The liquid ahead of the solidification front is modified by two combined phenomena, namely the expulsion of a water-saturated liquid and the arrival of fluids released by boiling and vesiculation. Because the system under study is a high-silica andesite (the AGV standard), the residual water-saturated liquid has the minimum composition of the granite system. This residual melt will be mixed with the pristine liquid ahead of the TBL leading to its fractionation. The change in the composition of the system has been modeled by using the general equation for *in-situ crystallization* [*Langmuir*, 1989]:

$$C_M = C_0\, F^{(f_A(E-1)/(f_A-1)} \qquad (4)$$

Where C_0 is the initial magma composition (in this case the standard AGV andesite), F is the fraction of melt (liquid / liquid + crystals), f_A is the fraction of liquid returned to the magma from the solidification front, and E is the partitioning coefficient, in this case taken as the ratio of the composition of the saturated liquid in the element of reference (C_{SL}) to the composition of magma in the same element of reference (C_M). The composition at any distance from the wall, after separation of the cumulate, requires integration over discrete increments of magma crystallization in which, F, E and f_A must be recalculated for every increment (Δ) of magma crystallization. We have introduced a restriction in the equation to calculate the amount of solid fraction at which the intercumulus liquid is expulsed from the crystal-rich mush. That solid fraction (1-F), or cumulate, at every discrete increment (Δ) is determined by the fraction of saturated liquid (X_{sl}), which is dictated by the ratio of the water content of magma (W_0) to the water content at saturation (Eq. 1). An iterative calculation at fixed increments of a unit volume of magma allows us to know the composition of the modified liquid ahead of the solidification front and, by simple mass balance, the composition of the solid residue. A plot of silica content of the modified liquid versus the fraction of remaining magma is shown in Fig. 5 for three values of initial water content (W_0) of 2, 3 and 5 wt% H_2O and at pressure of 5 kbar. Because water saturation is key in determining the fraction of saturated liquid that is available to modified the pristine liquid, it is clear that

the effect of fractionation is higher for systems containing the higher initial content of water (W_0). For values of $W_0 = 5$ the modified liquid reaches minimum silica values ($SiO_2 > 63$ wt%) of granitic rocks when only 20% of the whole magma is crystalized. However, magma with initial water content $W_0 = 3$ must crystalize about 50% of its initial volume to produce a fractionated liquid with $SiO_2 > 63$ wt%. Interestingly, the composition of cumulates remains almost constant compared with the continuous changing compositions of liquids. In nature, cumulates are represented by the fine-grained microgranular enclaves interpreted as autoliths, whose composition is very uniform within a particular pluton. Also notice that the most fractionated magma ($W_0 = 5$) yields the most mafic (less silicic) cumulates.

4 Magma Contamination by Country-Rock Assimilation

Contamination can be seen as an open-system mechanism of magma differentiation in the crust; as in the most general case contaminants are richer in evolved components, as alkali elements and silica, than the pristine magmas. Contamination may proceed in two ways that are not exclusive each other: (1) Assimilation of country rocks and (2) contamination by fluids derived from the host. Although contamination can be traced by means of isotopic ratios, source contamination can be difficult to distinguish from crustal-related processes. Fluids released by prograde metamorphic reactions in the thermal aureoles of plutons may expectedly contaminate the intruding magmas. However, this process is rarely identified in plutonic intrusions. Assimilation is the most documented process in crustal intrusions. Partial or total digestion of country rocks by the intruding magma is intrinsic to assimilation as an efficient mechanism that contributes to the contamination of magmas in the continental crust.

Although contamination by country-rock assimilation can be identified in geochemical diagrams, the intricacies of the process can be varied. The study of field relations in plutons is essential to constrain possible mechanisms. Experimental studies on magma–rock interactions are also relevant to test reactions and mineralogical implications and to assess the feasibility of assimilation on a regional scale. The two ways, field relations and experiments, are explored here on the basis of recently developed studies.

4.1 Field Relations Supporting Assimilation and Magma Contamination

Contamination of magmas with their host rocks can be identified easily by means of geochemical and isotopic relations. Paradoxically, although intermediate and silicic magmas have travelled long distances through the crust until their final storage in magma chambers or plutons and volcanic eruptions, not all silicic rocks are contaminated in the same extend and many of them maintain their pristine composition. There will be scenarios in which magma-host interactions are favored. Assimilation not only depends on the reactiveness between magma and country rocks but on the dynamics of ascent and emplacement and the rheological behavior of the two systems. An approach to the mechanical processes leading to assimilation of country rocks, and the consequent contamination of intruding magmas, can be made on the basis of field relations in areas on intense assimilation. A summary of these relations, based on relevant exposures of hybrid granites from the Gredos batholith (Central Spain), is shown in this section.

The Gredos batholith has been revealed during the last decade as one of the most outstanding and voluminous granitic exposures (more than 300 km in length and 60 km in width) to explore the interactions between intrusive magmas and a medium- to high-grade crustal sections. The batholith is mainly composed of Bt ±Crd granodiorites and monzogranites and minor amounts of basic rocks [*Scarrow et al.*, 2009] that depict a K-rich calc-alkaline suite characteristic of I-type post-collisional batholiths [*Castro*, 2019], emplaced during late D2 and D3 Variscan phases (320-290 Ma) [*Díaz Alvarado et al.*, 2013; *Díaz–Alvarado et al.*, 2011]. Detailed studies of the central area of the batholith have evidenced a laminar structure formed by mostly migmatitic host-rocks and intrusive layers. The conspicuous magmatic fabrics (foliations, lineations, folds and shear zones) are continued through the migmatitic structure of the host-rocks, which involve the synkinematic and sequential emplacement of intrusive magmas assisted by crustal-scale extensional shear zones, as have been revealed by structural and U–Pb geochronological studies [*Díaz Alvarado et al.*, 2013; *Díaz–Alvarado et al.*, 2012]. These characteristics of the emplacement process reinforced the long-lasting and close interaction between magmas and partially melted host-rocks that promoted the intense mingling and, finally, the chemical hybridization between both systems.

Geochemical, field and experimental evidences have shown that the hybridization between an intrusive magma and its host rock is an effective mechanism of magma

diversification during its ascent and emplacement [*Beard et al.*, 2005; *Díaz–Alvarado et al.*, 2011; *Erdmann et al.*, 2007]. The high diffusivity of some elements (e.g., the alkali elements) may favor the crystallization in the magma of particular phases, like Kfs, in areas far from the external contacts of the pluton with the host rocks [*Díaz–Alvarado*, 2017; *London et al.*, 2012]. However, Al-rich phases present in calc-alkaline granodiorites, like Crd and Grt, are diagnostic of assimilation processes and only appear in reactive domains where metasedimentary xenoliths were consumed or at least they lost their integrity (Fig. 6). In those cases, the original mineralogy of the xenoliths has been in part consumed by peritectic melting reactions to yield residual and peritectic minerals plus a granite melt, and in part is dispersed and camouflaged within the host magma. The only mineral species that can be considered exotic, in the sense that they are not present in the pristine magma, are the peritectic phases, cordierite or garnet. The amount of assimilated material in hybrid granites can be estimated by mass balance using the fraction of Crd [*Díaz–Alvarado et al.*, 2011; *Erdmann et al.*, 2007].

The main conditioning factor for this process is the effectiveness of the heterogeneous interaction process between the partially crystallized magma and the partially molten metasedimentary host rocks. The rheological characteristics of both systems tend to approach during the emplacement process, that is, while the migmatitic system increases its melt percentage and the magma continues its crystallization process (e.g. [*Vigneresse et al.*, 1996]. The driving forces of the emplacement process, including the stress state and the tectonic evolution of the crust, trigger the joint flow and deformation of the two systems, which yields a number of heterogeneous structures at all the scales [e.g. *Paterson et al.*, 2018; *Paterson et al.*, 1998], that are evidenced by the observed field relations (Fig. 7). Those structures can be ascribed to the following mechanisms of mechanical interaction between intruding magma and host rock: (1) Viscous folding; (2) Host-rock dragging; and (3) Migmatitic tearing apart. These structures can be ascribed to the following mechanisms of mechanical interaction between intruding magma and host rock: (1) Viscous folding (Fig. 7a–d); (2) Host-rock dragging (Fig. 7e); and (3) Migmatitic tearing apart (Fig. 7f).

4.1.1 Viscous Folding and Shearing

Complex fold geometries and distinct types of brittle and ductile shear zones are the most common structural features in migmatitic terrains [e.g. *Hopgood*, 1999]. In the case of a migmatitic crust intruded by a partially crystallized magma whose viscosities

543 approach during the evolution of both systems, the development of ductile deformation
544 structures such as folds and shears considerably increases the contact surface between
545 both systems and the isolation of host rock fragments within the intrusive magma (Fig.
546 7a, b). This process has been shown as a necessary condition for the complete
547 hybridization that results in contaminated magma [*Gogoi and Saikia*, 2018].
548 Assimilation through reaction of host-rock fragments implies the successive injection of
549 low crystal fraction magma batches, simultaneous development of assorted structures
550 under a viscous but evolutionary regime, melting reactions and chemical diffusion.
551 Therefore, deformation of the complex, composite system may be achieved through a
552 mechanism of viscous folding, which implies a viscosity contrast between magma and
553 host rock bodies (Fig. 7c, d) [e.g., *Biot*, 1961; *Chapple*, 1968; *Johnson and Fletcher*,
554 1994; *Ramberg*, 1961]. It is expected a viscosity switch along the interaction process,
555 such that the less viscous unit at the very beginning of the interaction process (i.e., the
556 intruding magma) becomes the more viscous one as it crystallizes, generating a very
557 complex and heterogeneous set of folding structures. This is evidenced by the complex
558 arrangement of Kfs megacryst fabrics that results firstly from the flow and interaction of
559 crystals in a fluid flow and the subsequent orientation of the same rigid particles
560 according to the contacts and the stress regime in a highly crystallized magma (Fig. 7a,
561 b).

562 4.2 Experiments on Contamination

563 One of the most outstanding criteria to identify a process of assimilation is the presence
564 of the peritectic phase Crd and/or Grt, which formed by fluid-absent (dehydration)
565 partial melting of pelitic metasediments, in a non-anatectic granodiorite or
566 monzogranite. A proof that Crd is not in equilibrium is such Ca-rich granite magma
567 composition is supplied by experiments with a Crd-bearing monzogranites, as these
568 failed to reproduce the Crd-bearing assemblage observed in nature [*García–Moreno et*
569 *al.*, 2017]. These experiments were performed using a synthetic glass with the
570 composition of a Crd-bearing peraluminous monzogranite of the Iberian Massif. This is
571 the Cabeza de Araya granite, whose composition is taken as representative of the so-
572 called “mixed granites” [*Capdevila et al.*, 1973], characterized by sharing features of
573 typical anatectic granites (S-type) and Bt-granodiorites (I-type). Crd-bearing
574 monzogranites appear in the Variscan belt of Iberia as isolated intrusions or as large
575 irregular domains inside calc-alkaline granodiorite batholiths. The origin of these

"atypical" granitic series has attracted much attention from petrologists over decades. We contend on the basis of geochemical, geological and experimental grounds that they are the products of crustal contamination by pelitic and semipelitic host rocks. In the case of Cabeza de Araya intrusion [*Corretgé*, 1971], the Crd-bearing monzogranites are located at the margins of the pluton. These represent the less evolved rocks that gradually transition into the central parts composed of two-mica granites and aplitic leucogranites. Emplacement age of the Cabeza de Araya granites obtained by SHRIMP lies between 308±1.5 Ma and 305±2 Ma for the different facies that compose the batholith [*Rubio–Ordóñez et al.*, 2016].

Large prismatic crystals (1 to 4 cm) of cordierite (Crd) are the most distinguishing feature of these "mixed" granites. The presence of Crd in this kind of granites has been interpreted as result of a peritectic reaction in the local domain of the xenoliths after wall-rock assimilation [*García–Moreno et al.*, 2017]. Interestingly, the outer zone of the pluton, in contact with the pelitic metasedimentary host, is the richer in Crd. The abundance of mafic microgranular enclaves (autoliths) and xenoliths is also greater in the margin zones compared to the inner parts. The inferences from field relations were tested with varied experimental designs using that and similar compositions.

Experimental approaches to test contamination processes are rooted in field and geochemical relationships in large composite batholiths, which point to physical and chemical interactions between the intruding magmas and its host rocks during ascent and emplacement [e.g. *Beard et al.*, 2005; *Díaz–Alvarado et al.*, 2011; *Erdmann et al.*, 2007; *London et al.*, 2012]. Different experimental procedures and strategies have led to relevant conclusions about diffusion and reactions between both subsystems.

4.2.1 Selective Assimilation Experiments

Experimental simulations in granodioritic and monzogranitic systems have shown that Crd or Grt do not precipitate during crystallization sequences, even when synthetic starting materials representing the whole composition of Crd- or Grt-bearing granitic rocks are used [*Díaz–Alvarado*, 2017; *García–Moreno et al.*, 2017]. The addition of aluminous phases to experimental capsules simulates the usual presence of And-, Sill- or/and Crd-rich restites in the migmatitic contact zones of intrusive bodies [*Acosta–Vigil et al.,* 2002*; Díaz–Alvarado et al.*, 2011]. Local domains are observed around xenocrysts in doped experiments, resembling reactive zones of high Al activity in melts around crystals or along layered contacts [*Acosta–Vigil et al.,* 2002*; Díaz–Alvarado et*

609 *al.*, 2011; *García–Moreno et al.*, 2017], but far from the conditions expected for the
610 massive crystallization of large euhedral diagnostic phases as Kfs and Grt or Crd. The
611 dissolution of exotic phases is goberned by the mineral reaction rates and diffusion
612 through the melt, besides other conditions as H_2O content and convection [*Acosta–Vigil*
613 *et al*., 2002, 2006]. Nonetheless, the above mentioned experiments show the resilience
614 of exotic xenocrysts in the intrusive magmas and the presence of local reactive domains.

615 4.2.2 Layered Experiments

616 Reaction at the interface between metasedimentary rocks and granitic melt
617 (granodioritic or haplogranitic depending on the experimental study) indicate that
618 homogenization took place for particular components as K, Na and H_2O between partial
619 melts at both sides of the interface [*Díaz–Alvarado*, 2017; *Erdmann et al.*, 2007;
620 *London et al.*, 2012]. The melt percentage increases in the pelitic system as it shifts to a
621 more haplogranitic composition (Erdmann, London op cit.). Two-layer experiments
622 represent static situations, being the crystallization of diagnostic phases restricted to a
623 narrow zone close to contact [*Erdmann et al.*, 2007; *London et al.*, 2012]. However, the
624 application of these results to the dynamic scenario of an ascent conduit, in which the
625 narrow zone of contaminated magma is continuously removed by flow, contamination
626 can be effective for large volumes of magma feeding an upper reservoir or pluton.
627 Contaminated granites can occupy large areas of zoned plutons. The process can demise
628 with time as the later magma pulses use the core of conduits and are prevented of
629 contamination. This, combined with increasing fractionation in conduits by
630 crystallization in a TBL (see above), can be a plausible explanation to many zoned
631 plutons in which the most contaminated and most mafic granites are disposed at the
632 outer rims, and the less contaminated and more felsic types are at the core.

633 4.2.3 Bulk-Assimilation Experiments

634 Bulk assimilation [*Beard et al.*, 2005] has been reproduced experimentally by
635 introduction of pelitic fragments into a granodiorite powder (Fig. 8) [*Díaz–Alvarado et*
636 *al.*, 2011], with significant implications for the linkage of this assimilation
637 mechanism with geochemical and mineralogical changes observed in large
638 batholiths [*Díaz–Alvarado et al.*, 2011; *Saito et al.*, 2007]. Partially disintegrated
639 xenoliths are still recognizable in the experimental runs (Fig. 8). Partial melts inside and

far from the xenolith domain still have important compositional differences (Al, Mg#) except for the alkalis, expelled from the xenoliths towards the granodioritic host, with the consequent enrichment in K and the early crystallization of Kfs, denoting a sort of mixing between the granodioritic and the xenolith-derived melts [*e.g. Díaz–Alvarado*, 2017; *Massota et al.,* 2018]. As in the layered experiments, euhedral Crd and Kfs are crystallized along the reactive xenolith area [*Díaz–Alvarado et al.*, 2011]. A dynamic scenario, as it was mentioned above, may contribute to disaggregation of xenoliths, leading to total digestion and dissemination of minerals within the intruding granite. Xenocrystic Pl, Bt or Qz are camouflaged in the contaminated magma, the euhedral Crd (Fig. 8) remaining as the only diagnostic mineral of the bulk assimilation, as described in natural examples (Fig. 6). However, a rapid segregation of interstitial melts in the crustal xenoliths may inhibit mineral–melt equilibrium and prompt the zonation of residual minerals [*Massota et al.,* 2018].

Although a significant percentage of the assimilated material gained by the contaminated magma is unrecognizable, it is possible to assess the extend of assimilation by measuring the abundance of Crd in the contaminated granites [*Díaz–Alvarado et al.*, 2011]. The results show that the assimilated material is approximately five times the proportion of Crd. This figure depends on the amount of pelitic components (Al, Fe, Mg) of the contaminant; the more pelitic the less fraction of contaminant in the final hybrid rock. Mass balance calculations and other approximations through Sr–Nd isotopic ratios are in agreement with these results [*Clarke et al.*, 2004; *Díaz–Alvarado et al.*, 2011; *Erdmann et al.*, 2007; *Fowler et al.*, 2001; *Ugidos and Recio*, 1993].

Batholithic examples, as the Gredos batholith (Iberian Massif), show that hybrid magmas may contain between 50% and 10% of assimilated material, depending on the proximity to the metasedimentary host, which fits well with the volume of Crd and Kfs estimated in the contaminated rocks [*Díaz–Alvarado et al.*, 2011]. The layered structure of the batholith and the coherent and tectonically induced viscous deformation of intrusive magmas and migmatitic host-rocks favored the increase of the contact surfaces between both subsystems, which has been proven essential for the efficacy of bulk assimilation. Besides, the sequential character of the emplacement process involves a long-lasting high-grade area in the host crust. The similar crystallization ages obtained from intrusive magmas and anatectic leucogranites [*Díaz Alvarado et al.*, 2013] formed and locally segregated in the migmatitic host-rocks, imply that both the intrusive

674 magmas and partially melted metasediments sustain a similar, albeit changing,
675 rheologic state during their heterogeneous and intense interaction, triggering the
676 geochemical and mineralogical changes that are characteristic of the assimilation
677 process and similar to the experimentally proved conditions that favor magma mixing
678 [*Laumonier et al.*, 2014a, b].

679 **5 Concluding remarks**

680 Differentiation and contamination are common processes in continental environments.
681 On a large extent the fractionated character of the continental crust with respect to the
682 underlying mantle is in sum the result of a protracted process of combined
683 differentiation and contamination. The latter is particularly relevant if available
684 contaminants are terrigenous metasediments, as these represent substantial geochemical
685 fractionation imposed by surface weathering. In most cases isotopic relations are good
686 indicators to distinguish between fractionation (closed systems) and contamination
687 (open systems). However, understanding the mechanisms that lead to magmas to
688 fractionate and/or to assimilate portions of country rocks, requires a deep knowledge of
689 complex magma systems. Two approaches, experimental and geological, have been
690 used in this paper to address the problem.
691 Field evidences from the Gredos batholith (Central Spain) support that assimilation of
692 pelitic metasediments caused the formation of Crd in local domains of the intrusive
693 granodiorite (calc-alkaline) magmas. Partial digestion of pelitic migmatites is common
694 at the contacts, where Crd formed by peritectic melting reactions in the pelites in the
695 course of xenolith disaggregation. These reactions are confirmed by means of
696 laboratory experiments using magma–pelite heterogeneous systems at conditions of
697 granodiorite emplacement of 850 °C and 4 kbar. Experiments reported that Crd is not
698 reproduced otherwise by crystallization of a glass with composition of a Crd-bearing
699 monzogranite. These results reinforce the idea that Crd in non-anatectic monzogranites
700 and granodiorites is in equilibrium within local subsystem created by assimilation of
701 country rock xenoliths. The existence of a thick (>5 km) sequence of Neoproterozoic
702 pelites and greywackes, as the regional host of Variscan batholiths, is the reason for the
703 conspicuous presence of Crd in varied types of granites from tonalites to monzogranites.
704 For the same reason, anatectic leucogranites with primordial (peritectic) Crd are so
705 abundant in Iberia. Granites emplaced into older igneous, either volcanic or plutonic,

host rocks are less prone to undergo contamination. This is the general case of the Cordilleran granite batholiths. In sum, the reactiveness of the host is a fundamental factor determining the feasibility of assimilation and contamination. Pelites are the most reactive systems and the formation of Crd in non-anatectic granites is diagnostic in such cases.

In regard of differentiation, our experiments in a thermal gradient or thermal boundary layer (TBL) are conclusive about the role of dissolved water in the magma in the separation of crystal and liquid, a necessary process to account for the origin of rock series that are linked to a parental magma by fractionation. Experiments with a natural andesite in horizontal capsules, not affected by gravitational processes, produce an interesting phenomenon that may help to understand geological and geochemical observations. This is we call *splitting*. Basically, a water-bearing magma crystallizing in a TBL is broken in two subsystems with a sharp boundary between them. One subsystem is formed by a crystal-rich aggregate, whose composition resembles the fine-grained microgranular enclaves that commonly appear in calc-alkaline batholiths, and the other subsystem is a fractionated liquid. The latter showing a composition that resembles that of the calc-alkaline granodiorites and granites. As enclaves are mostly autoliths, they represent magmas fragments with high crystal contents that are dragged from walls of ascent conduits. In this sense, we contend that conduits may have a primordial role to produce magmatic differentiation in the crust. We found that a plausible cause for liquid expulsion form the partially crystallized mush at the TBL is boiling and vesiculation, as water saturation is necessarily encountered at any point of the solidification front generated in a TBL. Vertical experiments, in which the thermal gradient and gravity acceleration vector are parallel, yield that crystal settling can be impeded by solid particle interactions, but that gravitational collapse of magma mushes from the top of the solidification front is possible.

Acknowledgements

This work is supported by the State Agency for Research (AEI) (Project: PGC2018–096534–B–I00). C.R. is grateful for her postdoctoral contract from the University of Huelva (Grant: Estrategia de Politíca Científica UHU 2016/2017).

References

Acosta–Vigil, A., D. London, T. A. Dewers, and G.B. Morgan VI (2002), Dissolution of corundum and andalusite in H_2O-saturated haplogranitic melts at 800 °C and 200 MPa: constraints on diffusivities and the generation of peraluminous melts. *Journal of Petrology, 43*, 1885-1908.

Acosta–Vigil, A., D. London, G.B. Morgan VI, and T. A. Dewers (2006), Dissolution of quartz, albite, and orthoclase in H_2O-saturated haplogranitic melt at 800 °C and 200 MPa: diffusive transport properties of granitic melts at crustal anatectic conditions. *Journal of Petrology, 47*, 231-254.

Allègre, C. J., and D. Ben Othman (1980), Nd-Sr isotopic relationship in granitoid rocks and continental crust development: a chemical approach to orogenesis, *Nature*, *286*, 335-341.

Bachmann, O., and G. W. Bergantz (2004), On the origin of crysytal-poor rhyolites: extracted from batholitic crystal mushes, *Journal of Petrology*, *45*, 1565-1582.

Bachmann, O., and C. Huber (2016), Silicic magma reservoirs in the Earth's crust, *American Mineralogist*, *101*(11), 2377-2404, doi:10.2138/am-2016-5675.

Bachmann, O., and C. Huber (2018), The Inner Workings of Crustal Distillation Columns; the Physical Mechanisms and Rates Controlling Phase Separation in Silicic Magma Reservoirs, *Journal of Petrology*, *60*(1), 3-18, doi:10.1093/petrology/egy103.

Bea, F., G. B. Fershtater, P. Montero, V. N. Smirnov, and J. F. Molina (2005), Deformation-driven differentiation of granitic magma: The Stepninsk pluton of the Uralides, Russia, *Lithos*, *81*(1-4), 209-233.

Beard, J. S., P. C. Ragland, and M. L. Crawford (2005), Reactive bulk assimilation: A model for crust-mantle mixing in silicic magmas, *Geology*, *33*(8), 681-684.

Biot, M. A. (1961), Theory of Folding of Stratified Viscoelastic Media and Its Implications in Tectonics and Orogenesis1, *GSA Bulletin*, *72*(11), 1595-1620, doi:10.1130/0016-7606(1961)72[1595:tofosv]2.0.co;2.

Bohrson, W. A., and F. J. Spera (2001), Energy-Constrained Open-System Magmatic Processes II: Application of Energy-Constrained Assimilation–Fractional Crystallization (EC-AFC) Model to Magmatic Systems, *Journal of Petrology*, *42*(5), 1019-1041, doi:10.1093/petrology/42.5.1019.

Bowen, N. L. (1922), The behaviour of inclusions in igneous magmas, *J Geol*, *30*, 513-570.

Bowen, N. L. (1928), The Evolution of Igneous Rocks. Princeton, New Jersey USA.

Brandeis, G., and C. Jaupart (1986), On the interaction between convection and crystallization in cooling magma chambers, *Earth and Planetary Science Letters*, *77*, 345-361.

774 Burgisser, A., and G. W. Bergantz (2011), A rapid mechanism to remobilize and
775 homogenize highly crystalline magma bodies, *Nature*, *471*, 212-217.

776 Burnham, C. W. (1979), The importance of volatile constituents, in *The evolution of the*
777 *igneous rocks*, edited by H. S. J. Yoder, pp. 439-482, Princeton University Press,
778 Princeton.

779 Capdevila, R., L. G. Corretgé, and P. Floor (1973), Les granitoides varisquies de la
780 Mesete Iberique, *Bulletin de la Société Géologique de France*, *7-15*, 209-228.

781 Castro, A. (2013), Tonalite-granodiorite suites as cotectic systems: A review of
782 experimental studies with applications to granitoid petrogenesis, *Earth-Science*
783 *Reviews*, *124*, 68-95, doi:10.1016/j.earscirev.2013.05.006.

784 Castro, A. (2019), The dual origin of I-type granites: the contribution from experiments,
785 *Geological Society, London, Special Publications*, *491*, SP491-2018-2110,
786 doi:10.1144/SP491-2018-110.

787 Castro, A., C. Fernández, C. Rodríguez, M. F. Pereira, and E. Aragón (2019),
788 Subduction to batholiths: Finding the bridge in North Patagonia, *Scientific Reports*
789 *(submitted)*.

790 Castro, A., et al. (2011), Petrology and SHRIMP U-Pb zircon geochronology of
791 Cordilleran granitoids of the Bariloche area, Argentina, *Journal of South American*
792 *Earth Sciences*, *doi:10.1016/j.jsames.2011.03.011*.

793 Chapple, W. M. (1968), A Mathematical Theory of Finite–Amplitude Rock–Folding,
794 *GSA Bulletin*, *79*(1), 47-68, doi:10.1130/0016-7606(1968)79[47:AMTOFR]2.0.CO;2.

795 Clarke, D. B., M. A. MacDonald, and S. Erdmann (2004), Chemical variation in Al_2O_3-
796 CaO-Na_2O-K_2O space: Controls on the peraluminosity of the South Mountain
797 Batholith, *Canadian Journal of Earth Sciences*, *41*(7), 785-798.

798 Corretgé, L. G. (1971), Estudio petrológico del batolito de Cabeza de Araya (Cáceres),
799 *Tesis Doctoral Univ. de Salamanca. P453*.

800 DePaolo, D. J. (1981), Trace element and isotopic effects of combined wallrock
801 assimilation and fractional crystallization, *Earth and Planetary Science Letters*, *53*(2),
802 189-202, doi:10.1016/0012-821X(81)90153-9.

803 Díaz Alvarado, J., C. Fernández, A. Castro, and I. Moreno-Ventas (2013), SHRIMP U–
804 Pb zircon geochronology and thermal modeling of multilayer granitoid intrusions:
805 Implications for the building and thermal evolution of the Central System batholith,
806 Iberian Massif, Spain, *Lithos*, *175–176*(0), 104-123,
807 doi:http://dx.doi.org/10.1016/j.lithos.2013.05.006.

808 Díaz-Alvarado, J. (2017), Experimental early crystallization of K-feldspar in granitic
809 systems. Implications on the origin of magmatic fabrics in granitic rocks, *Gologica*
810 *Acta*, *15*, 261-281.

Díaz-Alvarado, J., A. Castro, C. Fernández, and I. Moreno-Ventas (2011), Assessing bulk assimilation in cordierite-bearing granitoids from the central system batholith, Spain; experimental, geochemical and geochronological constraints, *Journal of Petrology*, *52*(2), 223-256, doi:10.1093/petrology/egq078.

Díaz-Alvarado, J., C. Fernández, M. Díaz-Azpiroz, A. Castro, and I. Moreno-Ventas (2012), Fabric evidence for granodiorite emplacement with extensional shear zones in the Variscan Gredos massif (Spanish Central System), *Journal of Structural Geology*, *42*, 74-90, doi:https://doi.org/10.1016/j.jsg.2012.06.012.

Erdmann, S., D. London, G. B. Morgan Vi, and D. B. Clarke (2007), The contamination of granitic magma by metasedimentary country-rock material: An experimental study, *Canadian Mineralogist*, *45*(1), 43-61.

Fernández, C., and A. Castro (2018), Mechanical and structural consequences of magma differentiation at ascent conduits: A possible origin for some mafic microgranular enclaves in granites, *Lithos*, *320-321*, 49-61, doi:10.1016/j.lithos.2018.09.004.

Flanagan, F. J. (1967), U.S. Geological Survey silicate rock standards, *Geochimica et Cosmochimica Acta*, *31*, 289-308.

Fowler, M. B., P. J. Henney, D. P. F. Darbyshire, and P. B. Greenwood (2001), Petrogenesis of high Ba-Sr granites: The Rogart pluton, Sutherland, *Journal of the Geological Society*, *158*(3), 521-534.

García-Moreno, O., L. G. Corretgé, F. Holtz, M. García-Arias, and C. Rodríguez (2017), Phase relations in the Cabeza de Araya cordierite monzogranite, Iberian Massif: implications for the formation of cordierite in a crystal mush, *Geologica Acta*, *15*(4), 337-359, doi: 10.1344/GeologicaActa2017.15.4.6.

Gelman, S. E., C. D. Deering, O. Bachmann, C. Huber, and F. J. Gutiérrez (2014), Identifying the crystal graveyards remaining after large silicic eruptions, *Earth and Planetary Science Letters*, *403*, 299-306, doi:http://dx.doi.org/10.1016/j.epsl.2014.07.005.

Glazner, A. F. (2007), Thermal limitations on incorporation of wall rock into magma, *Geology*, *35*(4), 319-322, doi:10.1130/G23134A.1.

Glazner, A. F. (2014), Magmatic life at low Reynolds number, *Geology*, *42*(11), 935-938, doi:10.1130/g36078.1.

Gogoi, B., and A. Saikia (2018), Role of viscous folding in magma mixing, *Chemical Geology*, *501*, 26-34, doi:https://doi.org/10.1016/j.chemgeo.2018.09.035.

Hawkesworth, C. J., and A. I. S. Kemp (2006), The differentiation and rates of generation of the continental crust, *Chemical Geology*, *226*(3-4), 134-143.

Hopgood, A. M. (1999), *Determination of Structural Successions in Migmatites and Gneisses*, 364 pp., Springer Science.

Huang, F., C. C. Lundstrom, J. Glessner, A. Ianno, A. Boudreau, J. Li, E. C. Ferré, S. Marshak, and J. DeFrates (2009), Chemical and isotopic fractionation of wet andesite in a temperature gradient: Experiments and models suggesting a new mechanism of magma differentiation, *Geochimica et Cosmochimica Acta*, *73*(3), 729-749.

Humphreys, M. C. S., and M. B. Holness (2010), Melt-rich segregations in the Skaergaard Marginal Border Series: Tearing of a vertical silicate mush, *Lithos*, *119*(3-4), 181-192, doi:10.1016/j.lithos.2010.06.006.

Johnson, A. M., and R. C. Fletcher (1994), *Folding of Viscous Layers*, Columbia University Press, New York.

Kemp, A. I. S., C. J. Hawkesworth, G. L. Foster, B. A. Paterson, J. D. Woodhead, J. M. Hergt, C. M. Gray, and M. J. Whitehouse (2007), Magmatic and crustal differentiation history of granitic rocks from Hf-O isotopes in zircon, *Science*, *315*(5814), 980-983.

Lake, E. T. (2013), Crystallization and saturation front propagation in silicic magma chambers, *Earth and Planetary Science Letters*, *383*(0), 182-193, doi:http://dx.doi.org/10.1016/j.epsl.2013.09.039.

Langmuir, C. H. (1989), Geochemical consequences of In situ crystallization, *Nature*, *340*, 199-205.

Laumonier, M., B. Scaillet, M. Pichavant, R. Champallier, J. Andujar, L. Arbaret (2014a), On the conditions of magma mixing and its bearing on andesite production in the crust. *Nature Communications, 5*, 5607.

Laumonier, M., B. Scaillet, L. Arbaret, R. Champallier (2014b), Experimental simulation of magma mixing at high pressure. *Lithos, 196*, 281-300.

Lee, C. T. A., X. Cheng, and U. Horodyskyj (2006), The development and refinement of continental arcs by primary basaltic magmatism, garnet pyroxenite accumulation, basaltic recharge and delamination: Insights from the Sierra Nevada, California, *Contributions to Mineralogy and Petrology*, *151*(2), 222-242.

Lee, C. T. A., and D. M. Morton (2015), High silica granites: Terminal porosity and crystal settling in shallow magma chambers, *Earth and Planetary Science Letters*, *409*, 23-31.

Lipman, P. W. (1988), Evolution of silicic magma in the upper crust: the mid-Tertiary Latir volcanic field and its cogenetic granitic batholith, northern New Mexico, USA, *Transactions of the Royal Society of Edinburgh, Earth Sciences*, *79*, 265-288.

London, D., G. B. Morgan, and A. Acosta-Vigil (2012), Experimental simulations of anatexis and assimilation involving metapelite and granitic melt, *Lithos*, *153*, 292-307, doi:https://doi.org/10.1016/j.lithos.2012.04.006.

Marsh, B.D. (1988), Crystal capture, sorting, and retention in convecting magma, *Geological Society of America Bulletin*, 100, 1720-1737.

886 Marsh, B. D. (2002), On bimodal differentiation by solidification front instability in
887 basaltic magmas, part 1: Basic mechanics, *Geochimica et Cosmochimica Acta*, *66*,
888 2211-2229.

889 Masotta, M., C. Freda, and M. Gaeta (2012), Origin of crystal-poor, differentiated
890 magmas: Insights from thermal gradient experiments, *Contributions to Mineralogy and*
891 *Petrology*, *163*(1), 49-65, doi:10.1007/s00410-011-0658-8.

892 Masotta, M., S. Mollo, M. Gaeta, and C. Freda (2016), Melt extraction in mush zones:
893 The case of crystal-rich enclaves at the Sabatini Volcanic District (central Italy), *Lithos*,
894 *248–251*, 288-292, doi:http://dx.doi.org/10.1016/j.lithos.2016.01.030.

895 McCulloch, M. T., and G. J. Wasserburg (1978), Sm-Nd and Rb-Sr chronology of
896 continental crust formation, *Science*, *200*, 1003-1011.

897 McKenzie, D. (1984), The Generation and Compaction of Partially Molten Rock,
898 *Journal of Petrology*, *25*(3), 713-765, doi:10.1093/petrology/25.3.713.

899 Michioka, H., and I. Sumita (2005), Rayleigh-Taylor instability of a particle packed
900 viscous fluid: Implications for a solidifying magma, *Geophysical Research Letters*, 32,
901 L03309, doi:10.1029/2004GL021827.

902 Namur, O., M. C. S. Humphreys, and M. B. Holness (2013), Lateral Reactive
903 Infiltration in a Vertical Gabbroic Crystal Mush, Skaergaard Intrusion, East Greenland,
904 *Journal of Petrology*, *54*(5), 985-1016, doi:10.1093/petrology/egt003.

905 Pankhurst, R. J., S. D. Weaver, F. Herve, and P. Larrondo (1999), Mesozoic-Cenozoic
906 evolution of the North Patagonian Batholith in Aysen, southern Chile, *Journal of the*
907 *Geological Society*, *156*(4), 673-694.

908 Paterson, S. R., K. Ardill, R. Vernon, and J. Žák (2018), A review of mesoscopic
909 magmatic structures and their potential for evaluating the hypersolidus evolution of
910 intrusive complexes, *Journal of Structural Geology*,
911 doi:https://doi.org/10.1016/j.jsg.2018.04.022.

912 Paterson, S., V. Memeti, R. Mundil, and J. Zák (2016), Repeated, multiscale, magmatic
913 erosion and recycling in an upper-crustal pluton: Implications for magma chamber
914 dynamics and magma volume estimates, *American Mineralogist*, *101*(10), 2176-2198,
915 doi:10.2138/am-2016-5576.

916 Paterson, S. R., T. K. Fowler, K. L. Schmidt, A. S. Yoshinobu, E. S. Yuan, and R. B.
917 Miller (1998), Interpreting magmatic fabric patterns in plutons, *Lithos*, *44*(1), 53-82,
918 doi:https://doi.org/10.1016/S0024-4937(98)00022-X.

919 Pistone, M., et al. (2015), Gas-driven filter pressing in magmas: Insights into in-situ
920 melt segregation from crystal mushes, *Geology*, *43*(8), 699-702, doi:10.1130/G36766.1.

921 Ramberg, H. (1961), Contact strain and folding instability of a multilayered body under
922 compression, *Geologische Rundshau 51*, 405-439.

Rodríguez, C., and A. Castro (2017), Silicic magma differentiation in ascent conduits. Experimental constraints, *Lithos*, *272-273*, 261-277, doi:http://dx.doi.org/10.1016/j.lithos.2016.12.017.

Rodríguez, C., and A. Castro (2019), Origins of mafic microgranular enclaves and enclave swarms in granites: Field and geochemical relations, *Geological Society of America Bulletin*, *131*(3/4), 635-660, doi:https://doi.org/10.1130/B32028.1.

Rubio-Ordóñez, A., O. García-Moreno, P. Montero, and F. Bea (2016), Nuevas aportaciones a la datación cronológica de los granitos de Cabeza de Araya, (Cáceres). , *Geotemas*, *16*(2), 43-46.

Saito, S., M. Arima, and T. Nakajima (2007), Hybridization of a shallow 'I-type' granitoid pluton and its host migmatite by magma-chamber wall collapse: The Tokuwa pluton, Central Japan, *Journal of Petrology*, *48*(1), 79-111.

Scarrow, J. H., J. F. Molina, F. Bea, and P. Montero (2009), Within-plate calc-alkaline rocks: Insights from alkaline mafic magma–peraluminous crustal melt hybrid appinites of the Central Iberian Variscan continental collision, *Lithos*, *110*, 50-64.

Shibano, Y., A. Namiki, and I. Sumita (2012), Experiments on upward migration of a liquid layer in a granular medium: Implications for a crystalline magma chamber, *Geochemistry, Geophysics, Geosystems*, 13, Q03007, doi:10.1029/2011GC003994.

Shibano, Y., I. Sumita, and A. Namiki (2013), A laboratory mdel for melting erosion of a magma chamber roof and the generation of a rhythmic layering, *Journal of Geophysical Research: Solid Earth*, 118, 4101-4116, doi:10.1002/jgrb.50295.

Thompson, A. B., L. Matile, and P. Ulmer (2002), Some thermal constraints on crustal assimilation during fractionation of hydrous, mantle-derived magmas with examples from Central Alpine Batholiths, *Journal of Petrology*, *43*(3), 403-422.

Ugidos, J. M., and C. Recio (1993), Origin of cordierite-bearing granites by assimilation in the Central Iberian Massif (CIM), Spain, *Chemical Geology*, *103*(1-4), 27-43.

Vigneresse, J. L., P. Barbey, and M. Cuney (1996), Rheological transitions during partial melting and crystallization with application to felsic magma segregation and transfer, *J. Petrol.*, *37*, 1579-1600.

Whitney, D. L., and B. W. Evans (2010), Abbreviations for names of rock-forming minerals, *American Mineralogist*, *95*(1), 185-187, doi:10.2138/am.2010.3371.

Paterson, S., V. Memeti, R. Mundil, and J. Zák (2016), Repeated, multiscale, magmatic erosion and recycling in an upper-crustal pluton: Implications for magma chamber dynamics and magma volume estimates, *American Mineralogist*, *101*(10), 2176-2198, doi:10.2138/am-2016-5576.

Žák, J., and S. R. Paterson (2010), Magmatic erosion of the solidification front during reintrusion: The eastern margin of the Tuolumne batholith, Sierra Nevada, California,

960 *International Journal of Earth Sciences*, *99*(4), 801-812, doi:10.1007/s00531-009-0423-
961 7.
962
963

964 **Captions to figures**

965

966 **Figure 1.** Geochemical variation plots, taken as proxies of phase diagrams, depicting
967 possible arrays of fractionation and contamination in calc-alkaline magma systems. (**a**)
968 The CaO–MgO diagram showing the curved array of experimental cotectic liquids
969 (orange dots) and their corresponding solid assemblages (blue hexagons) formed in
970 equilibrium at 3 kbar from an andesitic parental magma [*Castro 2013*]. The orange field
971 below the cotectic line represents the area of magmas that carry crystals from the
972 cumulate. The blue area represents the field crystal mushes that retain a liquid fraction
973 after extraction. Many rocks in batholiths plot in the two areas indicating that
974 fractionation is not perfect. Also shown as the lines of contamination with
975 metasedimentary rocks in case of open systems. (**b**) Projected space in the diagram
976 Opx–An–Or showing cotectic lines from experimental liquids at varied conditions of
977 pressure and water contents Rocks of the Gredos batholith in Central Spain are shown
978 as an example. These plot in part in the array of fractionation and in part in that of
979 assimilation (Modified from *Castro,* 2013]).

980 **Figure 2.** Electronic compositional images (backscattered electrons) and compositional
981 relations of a vertically arranged experimental run simulating magma crystallization in a
982 thermal gradient at 5 kbar. (**a**) Capsule section from a horizontally arranged run at the
983 same conditions of the vertical run (**b**). The thermal gradient of the assembly is shown
984 in (**b**) with a green curve and green diamonds from double thermocouple measurements.
985 The dashed curves L_0 in (**b**) represent the liquidus temperature taken from run CRH5
986 (See Fig. 4a). (**c**) Phase map of the bottom part of the vertical capsule (**b**). (**d**)
987 Compositional profiles of glasses (quenched liquid) along the vertical capsule. (**e**)
988 Interpretation of gravitational collapse of the upper carapace and liquid expulsion at the
989 bottom of the vertical capsule. The dashed curve represent the theoretical position of the
990 liquidus in the absence of gravity collapse (**a**).

991 **Figure 3.** Plot of critical crystallinity (X_{cc}=1–X_{sl}) versus initial water content (W_0) of a
992 granitic liquid using Eq. (3) at variable pressures from 3 to 6 kbar. The critical
993 crystallinity represents the crystal fraction at which the remaining liquid reaches water
994 saturation and boiling. The three zones of the solidification front (suspension, mush and
995 rigid crust) are marked using the boundaries given by [*Marsh*, 2002]. The most

favorable conditions to promote crystal–liquid separation by fluid-assisted filter pressing according to experiments [*Pistone et al.*, 2015] are also depicted.

Figure 4. (**a**) Mosaics of backscattered electron images from two polished sections of runs CRH5 and CRH4 with the AGV andesite (Rodríguez and Castro, 2018) using the thermal gradient imposed by the experimental assemblage. Initial conditions are P=5 kbar and T=1200 °C at the distance 0–3 mm from the thermocouple. CRH5 was quenched after 315 hours at the initial conditions. The liquidus (Cpx) is set approximately at 980 °C. In CRH4 T was dropped at the rate of 0.6 °C/hour during 308 hours (until 1016 °C at the thermocouple). The composition of glass (quenched liquid) at 2 mm of the thermocouple is more fractionated (richer in K2O and SiO2 and poorer in CaO and MgO) in CRH4 compared with CRH5, in which no gradient was applied. (**b**) Field photographs of partially dismembered autoliths from the Gredos batholith in Puente del Congosto (Central Spain).

Figure 5. Variation in the silica content of liquids (in a unit magma chamber) that are modified by influx of residual water-saturated liquid coming from the solidification front (thermal boundary layer) at the sidewalls. Liquid curves are calculated with Langmuir's equation [*Langmuir, 1989*] for in-situ crystallization (See text for further explanations).

Figure 6. Field relations of partially digested pelitic xenoliths enclosed in calc-alkaline monzogranites and granodiorites of the Gredos batholith (Central Spain). (**a**) Large xenolith of partially molten (migmatite) metasediments showing irregular contacts. (**b**) Detail of another xenolith showing the concentration of large Crd crystals (dark dots) around the contacts. (**c**) Sketch in two stages showing the possible digestion of xenoliths by peritectic melting reaction and the formation of Crd (green dots) and Kfs that appear finally disseminated in the contaminated zones. The arrival of K to the pristine granodiorite shifts the composition of the final contaminated magma to monzogranite.

Figure 7. Field examples (Gredos massif, Spain) of heterogeneous structures resulting from the interaction processes between a partially crystallized magma and a partially molten metasedimentary host rock. (**a**) to (**d**) are cases illustrating mechanisms of viscous folding and shearing. (**a**) and (**b**) Field photograph and interpretative sketch of complexly interleaved and folded sheets of migmatites, intrusive Bt granodiorite, and hybrid Kfs–Crd monzogranite. (**c**) and (**d**) Coeval folding (*f* is the axial trace) of metatexite and granodiorite intrusive sheets. Shear zones are also seen affecting the

system. (**e**) Sharp contact between the intrusive granodiorite (lower half of the photograph) and the migmatitic host rock (upper half) showing xenolithic fragments dragged by the intruding magma from its host rock. Inset depicts the final result of this process, with disaggregation of the metasedimentary xenoliths (melt + restitic and peritectic phases) within the granodiorite magma. (**f**) Tearing apart of migmatite mesosome from an intruding wedge of granodiorite magma promoted by the formation of a three-dimensional network of interconnected leucosome veins. Inset shows the individualization and disruption of sheets of mesosome and melanosome into the intruding magma. Grd: intrusive granodiorite. Mig: Migmatite. Leu: Leucosome.

Figure 8. Electronic compositional images (backscattered electrons) of experimental run products simulating reaction between a pelitic xenoliths and a granodiorite liquid, after *Díaz–Alvarado et al.* [*2011*]. (**a**) Section of the whole capsule showing the remnants of partially molten and dismembered xenoliths. (**b**), (**c**) and (**d**) Details of the same run product showing the formation of euhedral Crd and Kfs as peritectic phases.

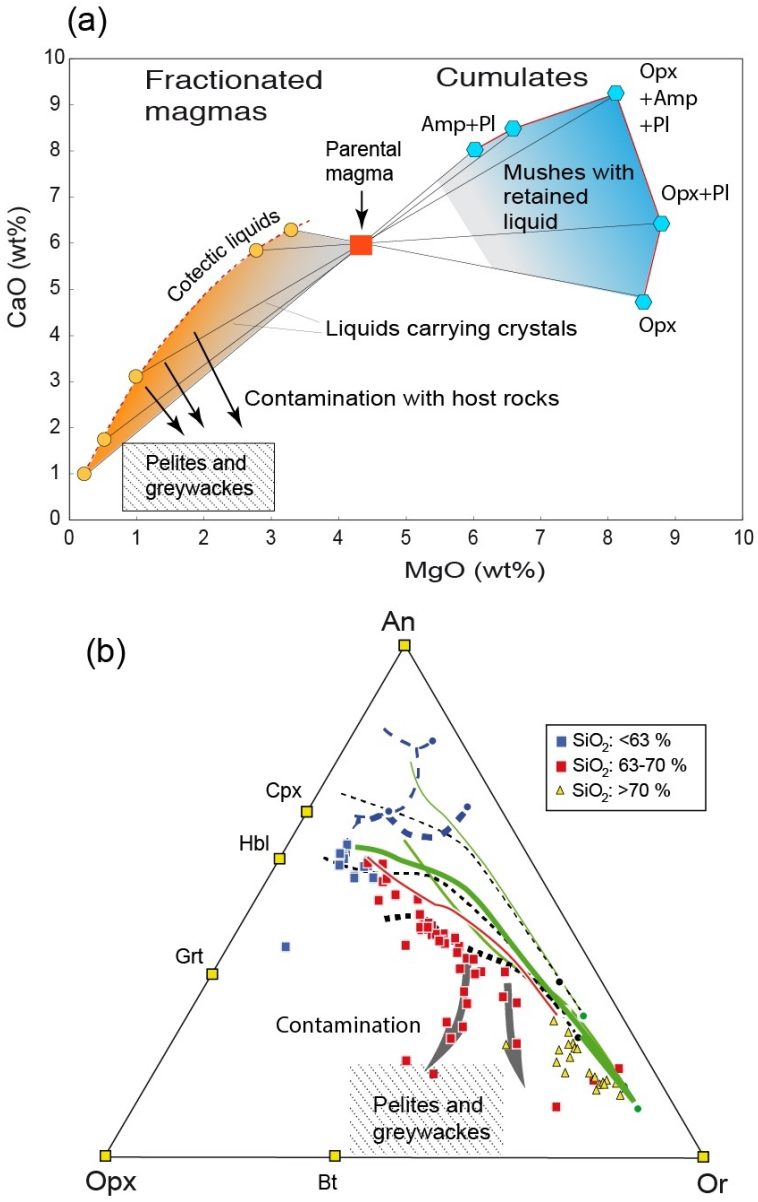

Figure 1 Geochemical variation plots, taken as proxies of phase diagrams, depicting possible arrays of fractionation and contamination in calc-alkaline magma systems. (a) The CaO-MgO diagram showing the curved array of experimental cotectic liquids (orange dots) and their corresponding solid assemblages (blue hexagons) formed in equilibrium at 3 kbar from an andesitic parental magma [Castro 2013]. The orange field below the cotectic line represents the area of magmas that carry crystals from the cumulate. The blue area represents the field crystal mushes that retain a liquid fraction after extraction. Many rocks in batholiths plot in the two areas indicating that fractionation is not perfect. Also shown as the lines of contamination with metasedimentary rocks in case of open systems. (b) Projected space in the diagram Opx-An-Or showing cotectic lines from experimental liquids at varied conditions of pressure and water contents Rocks of the Gredos batholith in Central Spain are shown as an example. These plot in part in the array of fractionation and in part in that of assimilation (Modified from Castro, 2013]).

142x226mm (150 x 150 DPI)

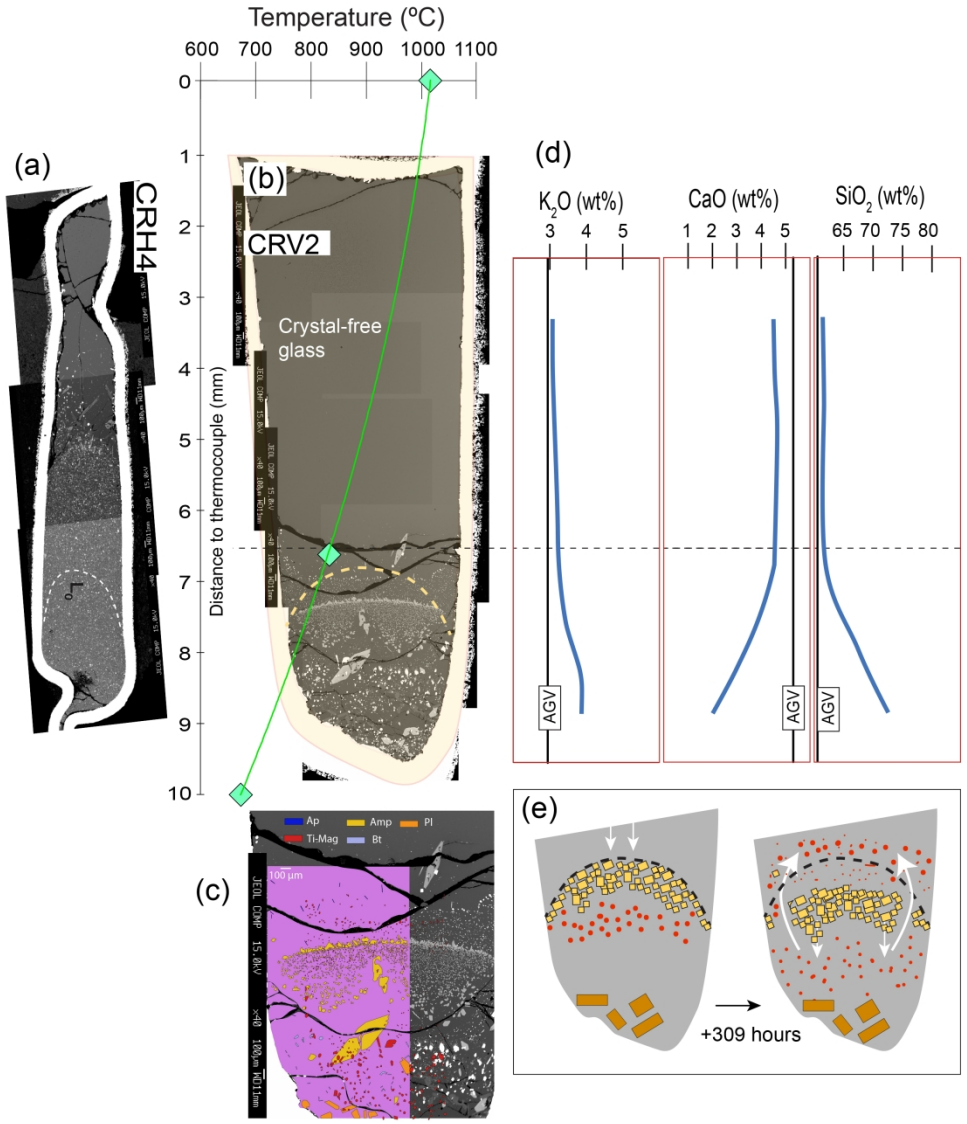

Figure 2 Electronic compositional images (backscattered electrons) and compositional relations of a vertically arranged experimental run simulating magma crystallization in a thermal gradient at 5 kbar [Rodríguez and Castro, 2017]. (a) Capsule section from a horizontally arranged run at the same conditions of the vertical run (b). The thermal gradient of the assembly is shown in (b) with a green curve and green diamonds from double thermocouple measurements. The dashed curves L0 in (b) represent the liquidus temperature taken from run CRH5 (See Fig. 4a). (c) Phase map of the bottom part of the vertical capsule (b). (d) Compositional profiles of glasses (quenched liquid) along the vertical capsule. (e) Interpretation of gravitational collapse of the upper carapace and liquid expulsion at the bottom of the vertical capsule. The dashed curve represent the theoretical position of the liquidus in the absence of gravity collapse (a).

246x277mm (300 x 300 DPI)

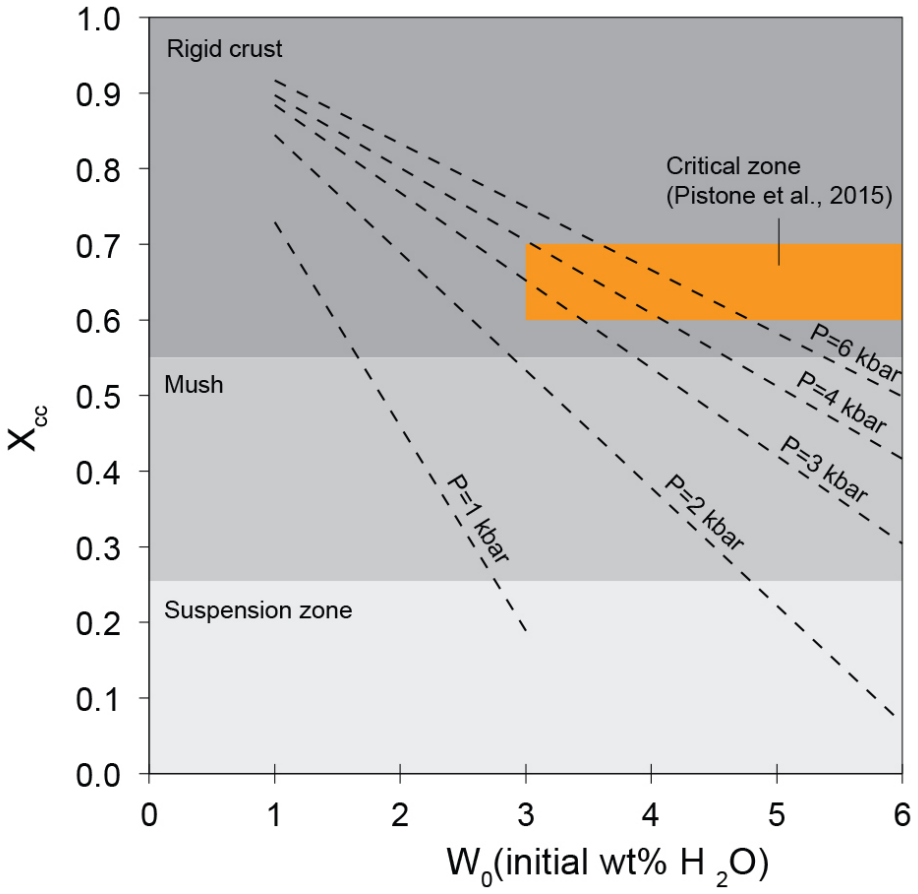

Figure 3 Plot of critical crystallinity (Xcc = 1–Xsl) versus initial water content (W0) of a granitic liquid using Eq. (3) at variable pressures from 3 to 6 kbar. The critical crystallinity represents the crystal fraction at which the remaining liquid reaches water saturation and boiling. The three zones of the solidification front (suspension, mush and rigid crust) are marked using the boundaries given by [Marsh, 2002]. The most favorable conditions to promote crystal-liquid separation by fluid-assisted filter pressing according to experiments [Pistone et al., 2015] are also depicted.

172x155mm (150 x 150 DPI)

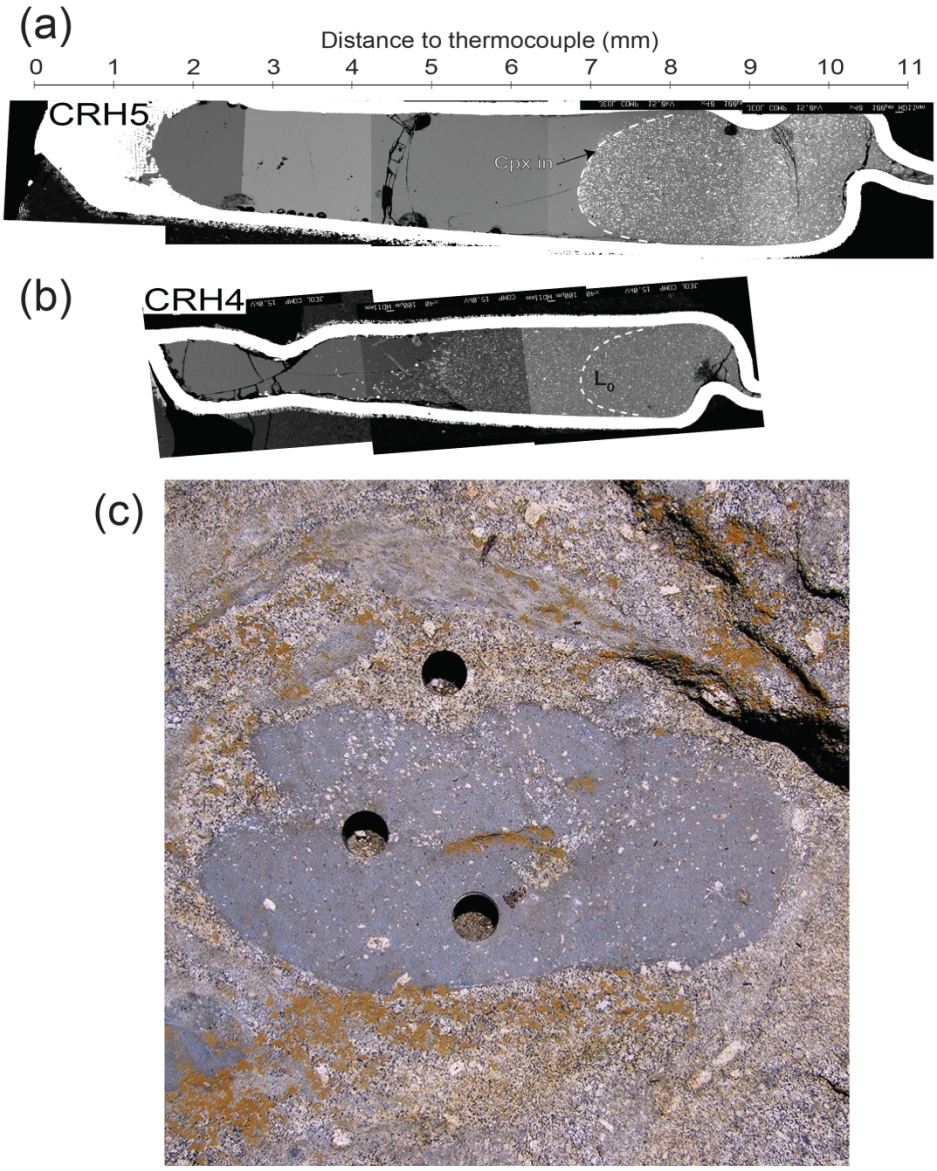

Figure 4 a) Mosaics of backscattered electron images from two polished sections of runs CRH5 and CRH4 with the AGV andesite (Rodríguez and Castro, 2017) using the thermal gradient imposed by the experimental assemblage. Initial conditions are P=5 kbar and T=1200 °C at the distance 0-3 mm from the thermocouple. CRH5 was quenched after 315 hours at the initial conditions. The liquidus (Cpx) is set approximately at 980 °C. In CRH4 T was dropen at the rate of 0.6 °C/hour during 308 hours (until 1016 °C at the thermocouple). The composition of glass (quenched liquid) at 2 mm of the thermocouple is more fractionated (richer in K2O and SiO2 and poorer in CaO and MgO) in CRH4 compared with CRH5, in which no gradient was applied.
b) Field photographs of partially dismembered autoliths from the Gredos batholith in Puente del Congosto (Central Spain).

192x226mm (300 x 300 DPI)

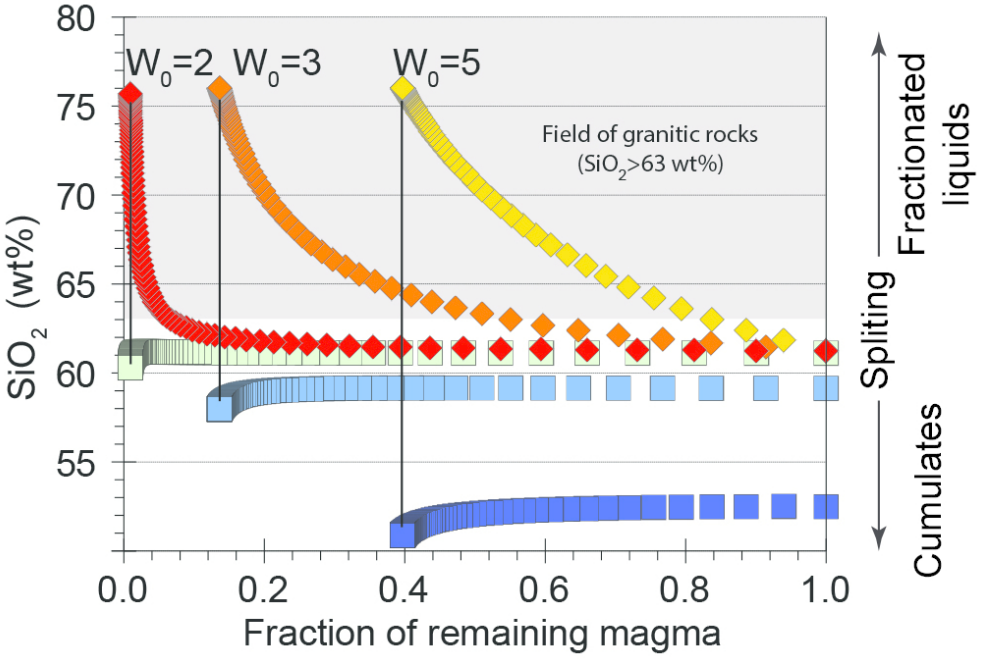

Figure 5 Variation in the silica content of liquids (in a unit magma chamber) that are modified by influx of residual water-saturated liquid coming from the solidification front (thermal boundary layer) at the sidewalls. Liquid curves are calculated with Langmuir's equation [Langmuir 1989] for in-situ crystallization (See text for further explanations).

172x117mm (150 x 150 DPI)

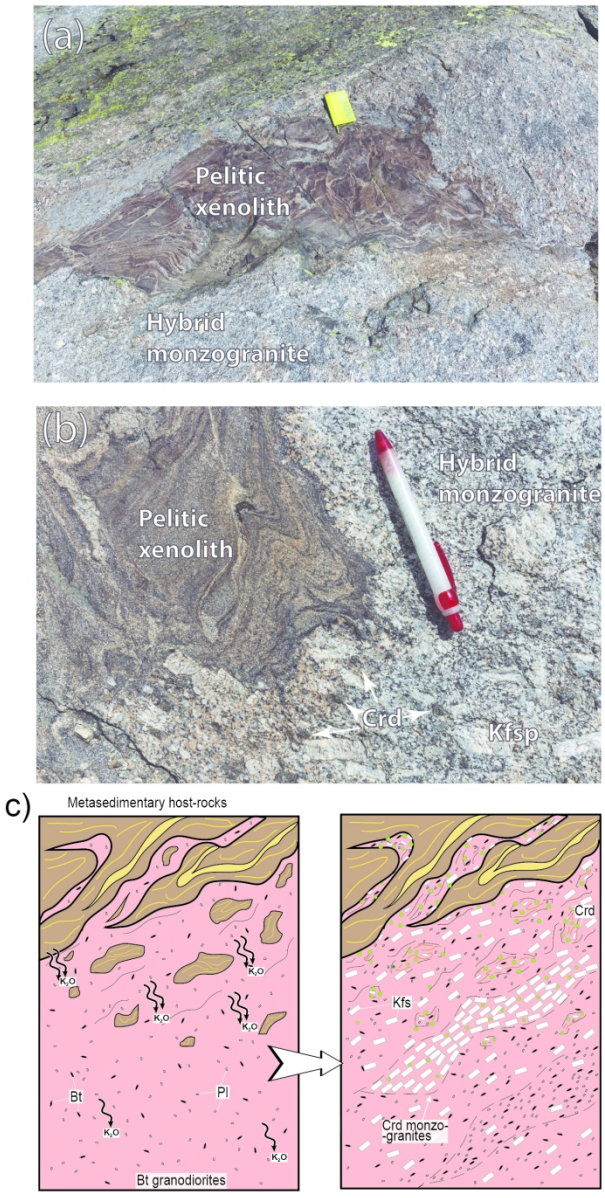

Figure 6 Field relations of partially digested pelitic xenoliths enclosed in calc-alkaline monzogranites and granodiorites of the Gredos batholith (Central Spain). (a) Large xenolith of partially molten (migmatite) metasediments showing irregular contacts. (b) Detail of another xenolith showing the concentration of large Crd crystals (dark dots) around the contacts. (c) Sketch in two stages showing the possible digestion of xenoliths by peritectic melting reaction and the formation of Crd (green dots) and Kfs that appear finally disseminated in the contaminated zones. The arrival of K to the pristine granodiorite shifts the composition of the final contaminated magma to monzogranite.

128x235mm (300 x 300 DPI)

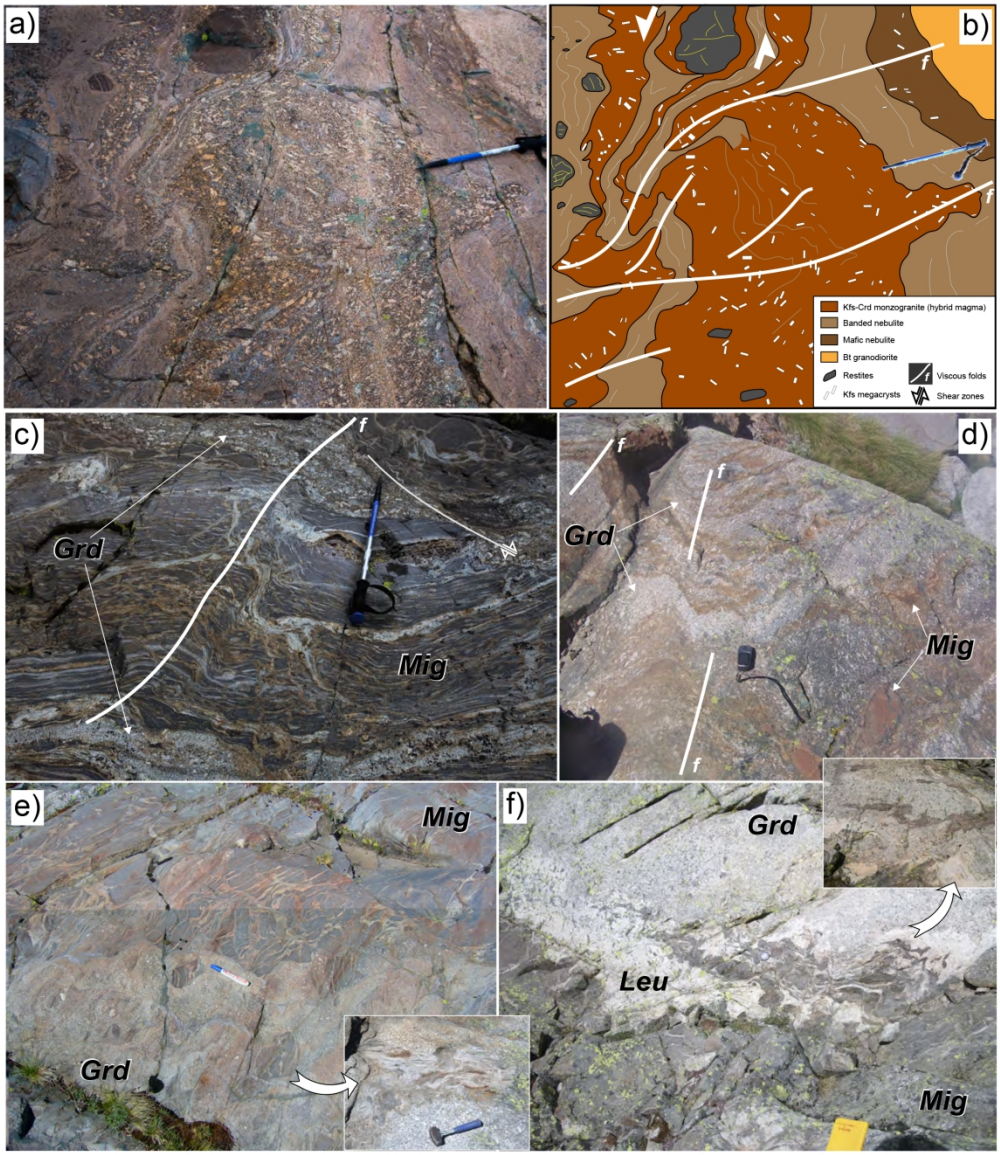

Figure 7 Field examples (Gredos massif, Spain) of heterogeneous structures resulting from the interaction processes between a partially crystallized magma and a partially molten metasedimentary host rock. A) to D) are cases illustrating mechanisms of viscous folding and shearing. A and B) Field photograph and interpretative sketch of complexly interleaved and folded sheets of migmatites, intrusive Bt granodiorite, and hybrid Kfs-Crd monzogranite. C and D) Coeval folding (f is the axial trace) of metatexite and granodiorite intrusive sheets. Shear zones are also seen affecting the system. E) Sharp contact between the intrusive granodiorite (lower half of the photograph) and the migmatitic host rock (upper half) showing xenolithic fragments dragged by the intruding magma from its host rock. Inset depicts the final result of this process, with disaggregation of the metasedimentary xenoliths (melt + restitic and peritectic phases) within the granodiorite magma. F) Tearing apart of migmatite mesosome from an intruding wedge of granodiorite magma promoted by the formation of a three-dimensional network of interconnected leucosome veins. Inset shows the individualization and disruption of sheets of mesosome and melanosome into the intruding magma. Grd: intrusive granodiorite. Mig: Migmatite. Leu: Leucosome.

209x243mm (300 x 300 DPI)

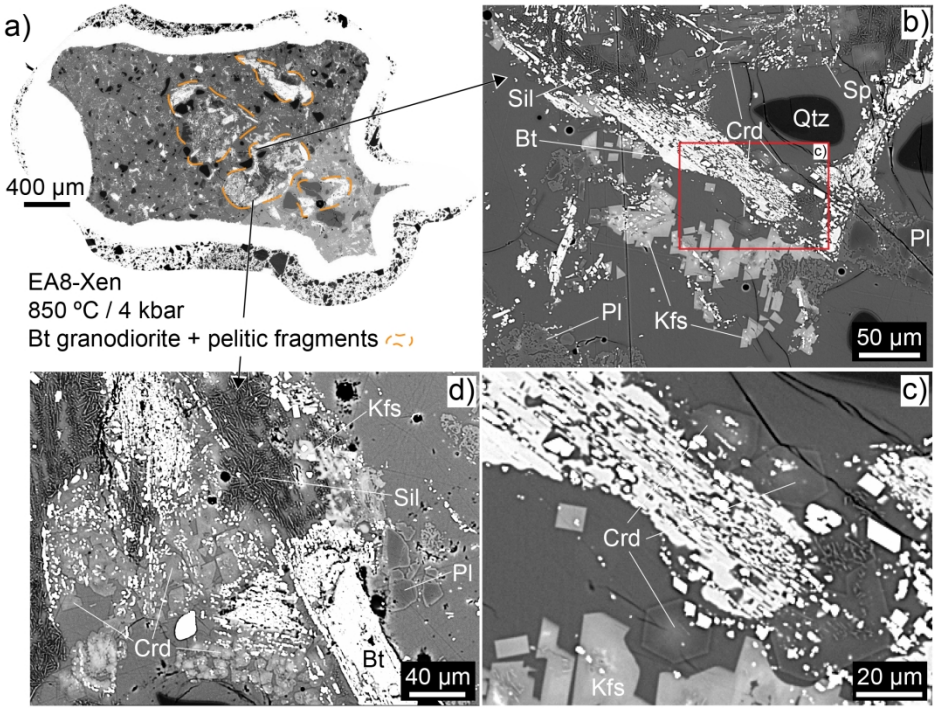

Figure 8 Electronic compositional images (backscattered electrons) of experimental run products simulating reaction between a pelitic xenoliths and a granodiorite liquid, after Díaz-Alvarado et al. [2011]. (a) Section of the whole capsule showing the remnants of partially molten and dismembered xenoliths. (b), (c) and (d) Details of the same run product showing the formation of euhedral Crd and Kfs as peritectic phases.

209x151mm (300 x 300 DPI)